



**HAL**  
open science

## Joint properties of a tool machining process to guarantee fluid-proof abilities

Camille Bataille, Raphaël Deltombe, Abdeljalil Jourani, Maxence Bigerelle

### ► To cite this version:

Camille Bataille, Raphaël Deltombe, Abdeljalil Jourani, Maxence Bigerelle. Joint properties of a tool machining process to guarantee fluid-proof abilities. *Surface Topography: Metrology and Properties*, 2017, 5 (4), pp.045002. 10.1088/2051-672X/aa8073 . hal-03461660

**HAL Id: hal-03461660**

**<https://uphf.hal.science/hal-03461660v1>**

Submitted on 9 Apr 2024

**HAL** is a multi-disciplinary open access archive for the deposit and dissemination of scientific research documents, whether they are published or not. The documents may come from teaching and research institutions in France or abroad, or from public or private research centers.

L'archive ouverte pluridisciplinaire **HAL**, est destinée au dépôt et à la diffusion de documents scientifiques de niveau recherche, publiés ou non, émanant des établissements d'enseignement et de recherche français ou étrangers, des laboratoires publics ou privés.

# Joint properties of a tool machining process to guarantee fluid-proof abilities

C Bataille<sup>\*</sup>, R Deltombe<sup>1</sup>, A Jourani<sup>2</sup> and M Bigerelle<sup>1</sup>

<sup>1</sup>LAMIH UMR CNRS 8201, Le Mont Houy, Valenciennes cedex 9 F59313, France

<sup>2</sup>Laboratoire Roberval, Centre de Recherches de Royallieu BP20259, Compiègne cedex 60205 France

\*Email: bataille.camille3@gmail.com

**Abstract.** This study addressed the impact of rod surface topography in contact with reciprocating seals. Rods were tooled with and without centreless grinding. All rods tooled with centreless grinding were fluid-proof, in contrast to rods tooled without centreless grinding that either had leaks or were fluid-proof. A method was developed to analyse the machining signature, and the software Mesrug<sup>TM</sup> was used in order to discriminate roughness parameters that can be used to characterize the sealing functionality. According to this surface roughness analysis, a fluid-proof rod tooled without centreless grinding presents aperiodic large plateaus, and the relevant roughness parameter for characterizing the sealing functionality is the density of summits  $S_{ds}$ . Increasing the density of summits counteracts leakage, which may be because motif decomposition integrates three topographical components: circularity (perpendicular long-wave roughness), longitudinal waviness, and roughness thanks to the Wolf pruning algorithm. A 3D analytical contact model was applied to analyse the contact area of each type of sample with the seal surface. This model provides a leakage probability, and the results were consistent with the interpretation of the topographical analysis.

**Keywords:** leak, surface roughness, superfinishing, contact modelling, reciprocating seals

## 1. Introduction

Leakage between cylindrical surfaces and seals is one of the most commonly encountered problems in industries. Many studies in different contexts (e.g., aeronautics, automotive) have analysed reciprocating seals in experiments and simulations, as shown by the historical reviews of Nikas [1] and Nau [2]. The studied system has a complex behaviour because of the number of variables that can potentially affect the contact sealing performance [3]. This paper focuses on the impact of surface roughness on the sealing contact performance. Many past studies considered seal and rod surfaces as smooth until Kanters and Vissler [4] analysed the impact of the surface roughness of rods and seals on the coefficient of friction and proved that the surface roughness is significant to the seal lubrication. Furthermore, Nikas [5] realised a numerical model that is able to simulate the sealing contact of a rectangular elastomeric seals for reciprocating piston rods by considering the rod and seal surface roughness in mixed lubrication regimes. Other researchers such as Crudu *et al.* [6] and Huang *et al.* [7] now consider the surface roughness of reciprocating seals in numerical models.

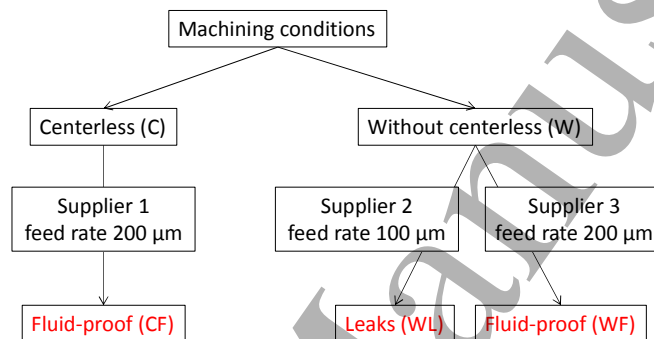
Rods are tooled by a turning process, which generates anisotropic roughness. Therefore, the direction of leakage is closely related to the anisotropy of the topographical structure, which induces an anisotropic flow. The aim of the present study was to characterize the sealing functionality according to the rod surface topography under different machining conditions. All tested rods were treated with a PVD coating, which has been investigated as part of research on hard chromium substitution [8].

To complete the topography analysis, a contact simulation was performed to determine the leakage mechanism. The objective was to characterize the influence of rod surface roughness on the fluid-proof abilities of a sliding contact.

## 2. Materials and methods

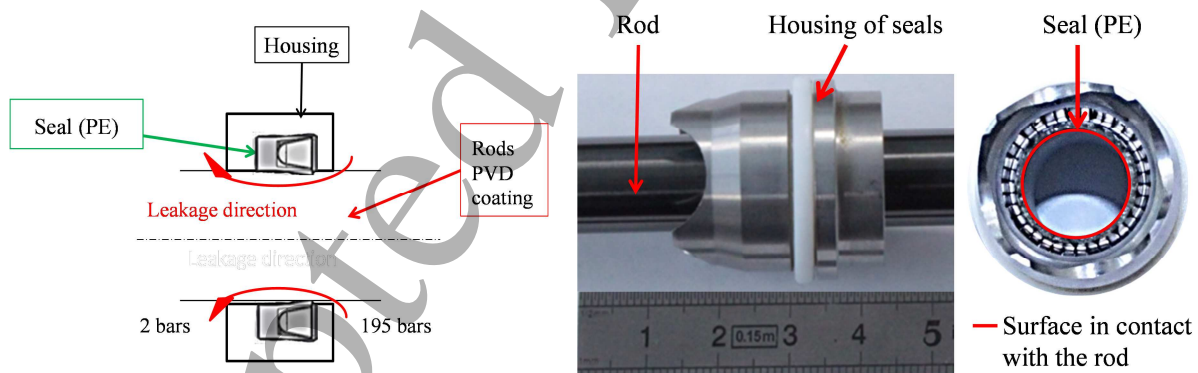
### 2.1. Experimental conditions

Rods (i.e. plunger of a pump) were tooled under different conditions before PVD coating, as shown in figure 1: with centreless grinding (C) and without centreless grinding (W) using two different tooling machines. Rods tooled without centreless grinding had different machining feed rates (100 and 200  $\mu\text{m}$ ), and rods tooled without centreless grinding had a step-over at 200  $\mu\text{m}$ . Surfaces were super-finished by a grinding process before physical vapour deposition was performed to increase the wear resistance. Three suppliers were used for the rods. The first supplier tooled rods without centreless grinding and with leaks (WL), the second supplier tooled rods without centreless grinding that were fluid-proof (WF), and the third supplier tooled rods with centreless grinding that were fluid-proof (CF). Three samples from each production batch were analysed.



**Figure 1.** Tooling conditions.

Rods were in contact with a lip seal based on polyethylene Avalon 42, as shown in figure 2. The fluid pressure was 195 bar, and the air pressure was 6 bar. The fluid volume was 25  $\text{cm}^3$  per cycle (30 cycles/min).



**Figure 2.** Studied system: (left) technical drawing, (right) system picture.

### 2.2. Roughness measurement

In order to compare the surface topographies of each sample's configuration, surfaces were measured with a white light interferometer (NewView 7300, Zygo<sup>TM</sup>). All measurements were performed with a 0.10 nm vertical resolution. Rod surfaces were analysed along their axes following several generatrices. To perform this task, the rods were placed on a V-shape support with a graduated washer at angle intervals of 36°. A reference point was placed on the head of the rod in order to control the angular position. Two different measurement procedures were established in order to analyse the surface topography at different scales:

- Macroscale measurement was performed along the axis of the rod every 40 mm and every 36°.

- The microscale measurement was performed along the axis of the rod every 24 mm and every 36°.
  - The nanoscale measurement included a single measure comprising local-scale measurements.
- Table 1 presents the details of the multi-scale measurement.

**Table 1.** Measurement details.

Macro-scale (Form)	Micro-scale (Waviness)	Nano-scale (Roughness)
<p><b>Objective: 5×</b>            Size: 41996 <math>\mu\text{m}</math> <math>\times</math> 784 <math>\mu\text{m}</math>            (1 <math>\times</math> 36 single surface)            9534 points <math>\times</math> 179 lines            Single measurement size:            0.286 mm <math>\times</math> 0.215 mm</p>	<p><b>Objective: 20×</b>            Size: 4810 <math>\mu\text{m}</math> <math>\times</math> 1015 <math>\mu\text{m}</math>            (5 <math>\times</math> 36 single surface)            8803 points <math>\times</math> 1858 lines            Single measurement size:            0.286 <math>\times</math> 0.215 mm</p>	<p><b>Objective: 20×</b>            Size: 286 <math>\mu\text{m}</math> <math>\times</math> 215 <math>\mu\text{m}</math>            Single surface            640 points <math>\times</math> 480 lines            Single measurement size:            0.286 <math>\times</math> 0.215 mm</p>
<b>Lateral resolution: 2.19 <math>\mu\text{m}</math></b>	<b>Lateral resolution: 0.71 <math>\mu\text{m}</math></b>	<b>Lateral resolution: 0.71 <math>\mu\text{m}</math></b>

### 2.3. Measurement treatment

All measurements were treated before analysis to obtain reliable results:

- Polynomial fitting was applied to define the measurement references. A third-degree polynomial fitting was used to delete the surface form.

- Less than 0.5% of the data were not measured and were interpolated by spline functions.

The software Mesrug™ [9, 10] was used for all surface treatment, the calculation of surface roughness parameters and the relevance analysis in order to discriminate the best roughness parameter for characterizing the sealing functionality. The method used to find the most relevant parameter was described by Bigerelle *et al.* [11] and merges discriminant analysis [12] with a bootstrap method [13].

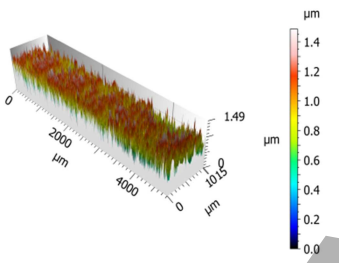
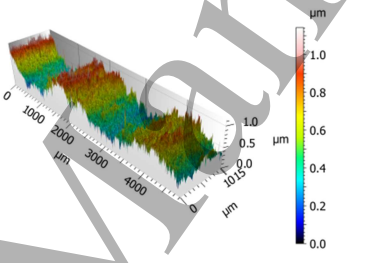
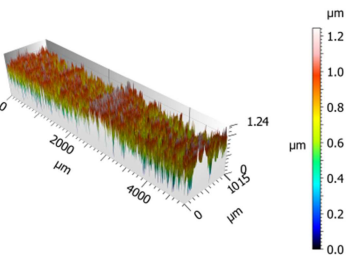
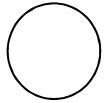

## 3. Results

### 3.1. Machining signature of each type of sample

All surface topographies were compared to each other in order to qualitatively differentiate between leaking and fluid-proof surfaces. The machining signature and surface topography of each type of sample were compared with each other. Table 2 summarizes the topographical characteristics of all samples under the experimental conditions. First, a shape difference was detected in samples machined without centreless grinding. Núñez *et al.* [14] explained that the shape defects obtained during the machining process without centreless grinding are due to the vibration of the machined pieces.

However, these defects do not explain the fluid-proof ability of 80% of the rods tooled without centreless grinding. Therefore, the topographical characteristics of each sample were studied. The topographies of the WL and CF rods were similar and had periodic stripes in the orthogonal direction of the leakage. They differed in the shape defects and machining periodicity. In contrast, the WF samples exhibited a different topographical structure of high and wide non-periodic plateaus. Visualizing the topographical differences for each type of sample was insufficient for understanding the origin of the leakage. The sample roughness parameters were then analysed to detect a roughness parameter that can be used to characterize the leakage function.

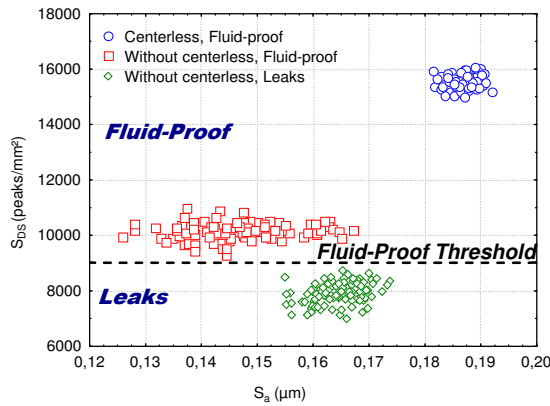
**Table 2.** Topography comparison of each rod type.

Sample	Centreless grinding and fluid-proof (CF)	Without centreless grinding and fluid-proof (WF)	Without centreless grinding and with leaks (WL)
<b>Roughness</b>	<p><b>Machining signature, T = 200 <math>\mu\text{m}</math></b>            Roughness signature sometimes deleted by the superfinishing process</p>	<p><b>Peaks with periodicity, T = 200 <math>\mu\text{m}</math></b>  <b>Large and high plateau structure</b>            Plateau amplitude (between 1 and 2 <math>\mu\text{m}</math>) represents 80% of the roughness amplitude.            Signal variation wavelength is between 2 and 3 mm.</p>	<p><b>Machining signature, T = 100 <math>\mu\text{m}</math></b>            Machining roughness amplitude represents 50% of the surface roughness.</p>
<b>Topography</b>			
<b>Form</b>	<p>No roundness default:</p> 	<p>Rod shape default (roundness):</p> 	

### 3.2. Sealing characterization

Relevance analysis of roughness parameters (ISO 11562-1996 [15] and ASME B46.1-1995 [16]) was performed to characterize the best roughness parameter depending on the sealing function. This relevance analysis combined discriminant analysis with a bootstrap method. These operations were performed by using the Mesrug™ software [9]. The discriminant analysis indicated that the most relevant parameter for characterizing the leakage is the  $S_{ds}$  roughness parameter, which represents the density of summits. In contrast, the roughness parameter  $S_a$  cannot be used to distinguish between leaking and fluid-proof rods. Figure 3 shows the relationship between the two roughness parameters for each type of rod.





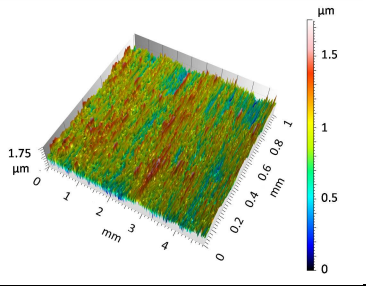
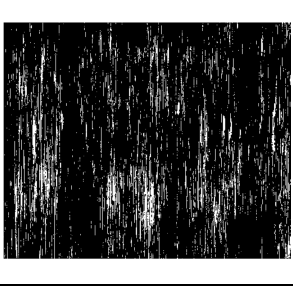
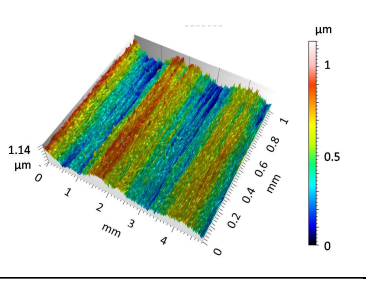

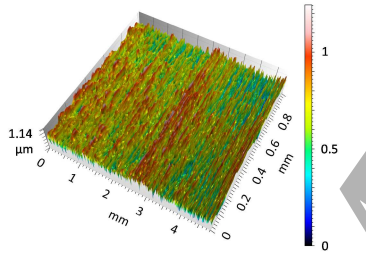
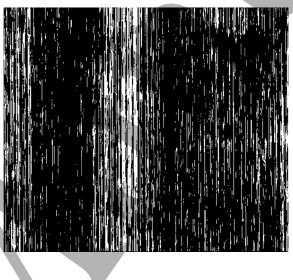
**Figure 3.** Sds according to  $S_a$  for each type of rod studied.

The relevancy threshold is represented by a black horizontal dashed line ( $S_{ds} = 9000$  peaks/mm<sup>2</sup>). Remarkably,  $S_a$  was not relevant in contrast to  $S_{ds}$ . The latter was found to be the most relevant roughness parameter for characterizing the leakage. Thus,  $S_{ds}$  is the only roughness parameter that can be used to distinguish between leaking and fluid-proof samples. All other relevant parameters could only distinguish between each type of sample without taking the sealing function into consideration. According to figure 3, the most relevant roughness parameter for characterizing the fluid-proof ability is  $S_{ds}$ . The isotropy parameter can also distinguish the leakage phenomenon but is not as relevant as  $S_{ds}$  [17]. According to figure 3, when  $S_{ds}$  is greater than 9000 peaks/mm<sup>2</sup>, all samples are fluid-proof. The topography is highly repeatable (appendix A). This means that the leakage is not due to the heterogeneity of the roughness along the rod axis nor the roughness variation along the rod in circular coordinates.

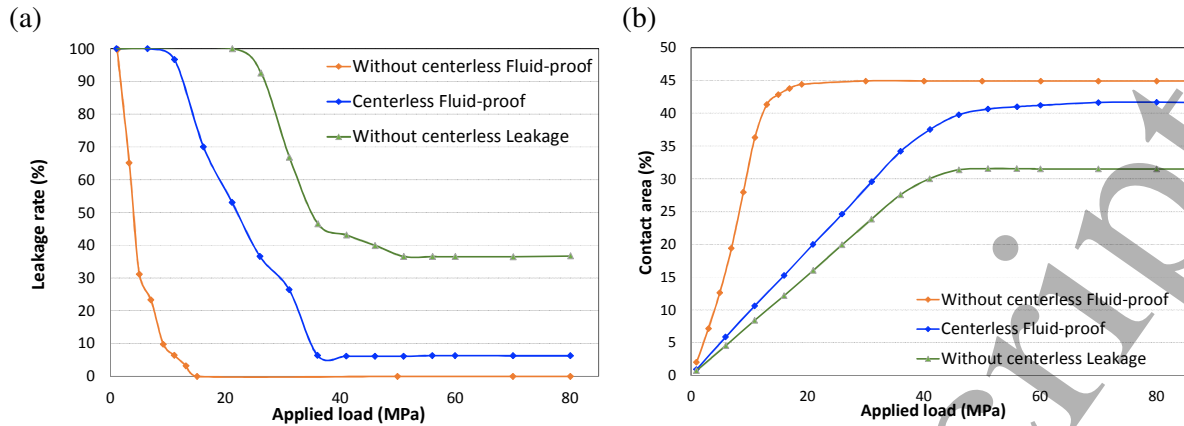
### 3.3. Contact simulation

A contact simulation analysis was performed in order to understand how the  $S_{ds}$  surface roughness parameter can characterize the fluid-proof ability of surfaces. The impact of the different topographies of each type of sample on the contact distribution was examined. A contact simulation based on the method developed by Jourani *et al.* [18, 19] was performed to compare the contact areas of both types of rods and seals. On a microscopic scale, this simulation helped demonstrate the mechanism for the leakage. The seal rigidity was considered infinite to compare the impact of rod surface roughness differences on the contact distribution. In total, 150 simulations of 150 roughness maps were performed for each type of samples. Table 3 presents the simulation results of three examples.

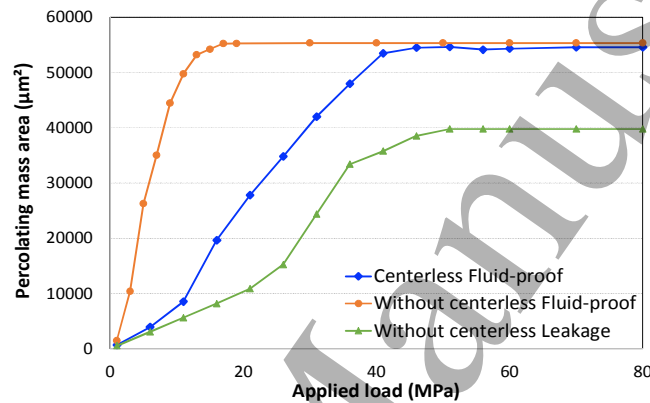
**Table 3.** Simulation analysis of each type of rod at the micro-scale; black: fluid, white: contact.

		Topography	Contact area	Observations
Centreless grinding	Fluid-proof (CF)			No fence
Without centreless grinding	Fluid-proof (WF)			Macroscopic fences
Without centreless grinding	Leak (WL)			Microscopic fences

Rods tooled with centreless grinding (CF) showed no fence, in contrast with both rods tooled without centreless grinding (WF and WL). The WF surface featured many fences orthogonal to the direction of the rod movement (also corresponding to the fluid movement), which made it fluid-proof. Larger and higher barriers were observed on the WF rods compared to the WL rods. The contact area and leakage path were calculated under fixed pressures. The 150 simulations were used to calculate the leakage probability. This probability represents the proportion of leaking rods for the total number of simulated surfaces, as shown in figure 4a. According to the simulations, the leaking rods tooled without centreless grinding showed a leakage probability of 37% at an applied load of 50 MPa; fluid-proof rods tooled with centreless grinding showed a leakage probability of 7% at an applied load of 40 MPa; and fluid-proof rods tooled without centreless grinding had a leakage probability of zero at an applied load of 15 MPa. The last type of rod is the most affordable. As proven by the simulation results, figure 4b shows the contact area evolution of each type of rod surface according to the contact pressure. The leaking rods had a contact area with the seal of 32% at an applied load of 50 MPa, which was less than that of the fluid-proof rods. The fluid-proof rods tooled with centreless grinding had a contact area of 42%. Fluid-proof rods tooled without centreless grinding had the most contact area (up to 45%) regardless of the contact pressure. To understand the leakage, observing the percolation through the surface peaks is important.



**Figure 4.** (a) Leakage rate load according to the contact pressure. (b) Contact area according to the contact pressure.



**Figure 5.** Most significant percolating mass area according to the contact pressure.

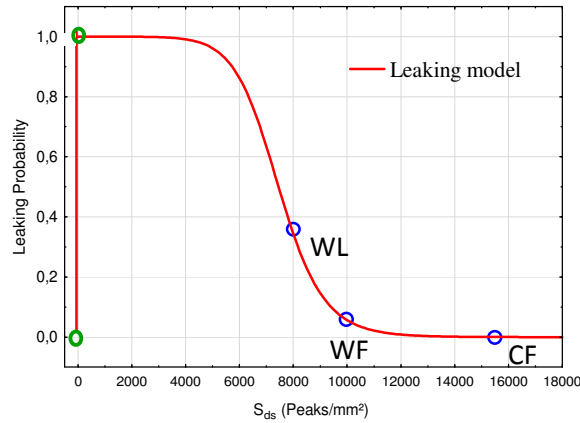
Figure 5 shows the most significant percolating mass that could pass through the contact between the seal and rod surface according to the pressure. The most significant percolating mass represents the largest cluster, which was formed when the points of the sample were connected, that could counteract the leakage [20]. The most significant percolating mass that could counteract the leakage was calculated according to the pressure. The more significant a percolating mass, the less fluid that can go through the contact, and the less significant the leakage. Leaking rods tooled without centreless grinding had substantially smaller percolating masses.

In summary, the simulation results showed that rods can be classified in term of the best sealing performance. The most effective type of rod was WF, and the worst was WL. CF can control the sealing performance but not as effectively as WF.

#### 4. Discussion

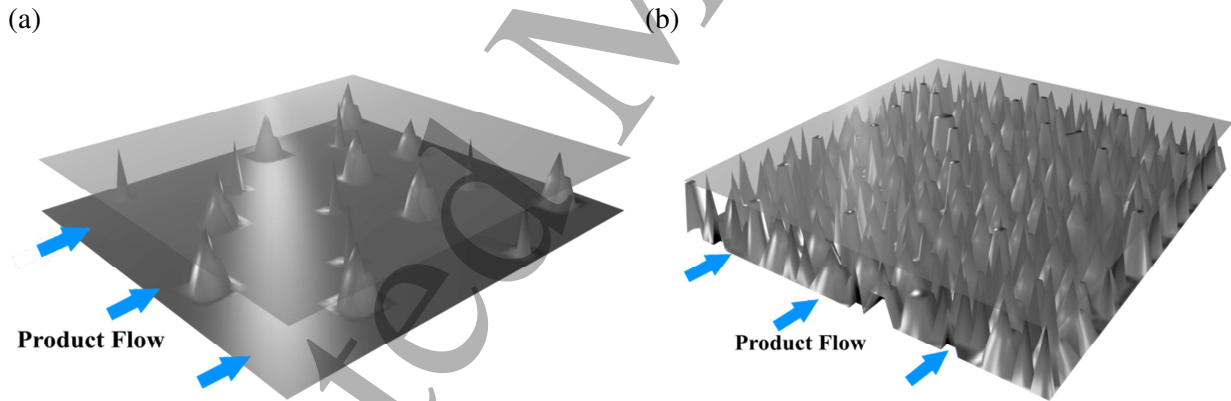
The influence of topography differences induced by their respective machining processes was examined. Regarding the leakage of rods, the discriminant analysis (figure 3) indicated that the peak density  $S_d$  is the most relevant parameter for characterizing the leakage. Based on the roughness measurements and simulations, a sigmoidal model is proposed. For a few peaks on the surface ( $S_d \approx 0$  peaks/ $\text{mm}^2$ ), the leakage probability is equal to unity. An infinite number of peaks decrease the leakage probability to 0. As shown by Bottiglione *et al.* [20], when a fluid is present, the percolating mass follows a power law. Therefore, increasing  $S_d$  will increase the number of percolating sites, which leads to the sigmoidal shown in figure 6.





**Figure 6.** Leakage probability according to  $S_{ds}$

First, a contact between two surfaces without roughness ( $S_{ds} = 0$  peaks/mm<sup>2</sup>), which is represented by the green points in figure 6, will not leak. However, according to Papatheodorou and Hannifin [21], a rod with an excessively smooth surface roughness will leak rapidly because of a higher friction coefficient, which can lead to wearing of the seal and consequently leakage. If few peaks are located on the surface, as suggested by figure 7a, a seal will appear on the contact. This case is represented by the green points at the leakage probability equal to 1 in figure 6. The simulation results showed that the leakage will decrease with increasing  $S_{ds}$  until there are enough peaks to make the contact fluid-proof, as shown by the blue points in figure 6. Figure 7b shows the increasing number of peaks at the contact that counteract the leakage. However, all simulations showed that the WF rods clearly performed better than the CF and WL rods. The most important difference between the WF rods and the other samples is the long quasi-period of waviness. This structure increases the global contact pressure. The contact pressure is concentrated on the plateaus, which increases the contact area and improves the percolation between these surfaces. Figure 7c provides an overview of this phenomenon.



(a)

(b)

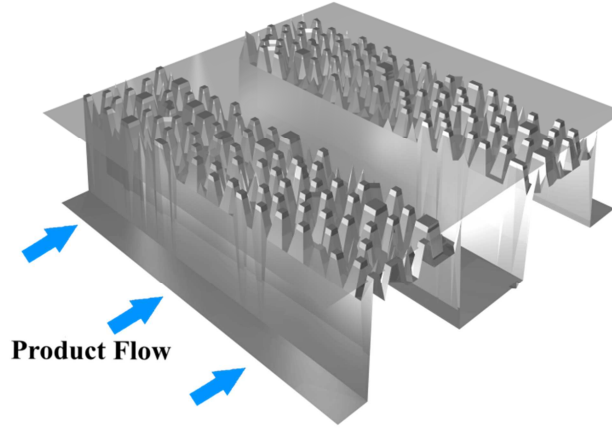
Product Flow

Product Flow

Accepted Manuscript

2  
3  
4  
5  
6  
7  
8  
9  
10  
11  
12  
13  
14  
15  
16  
17  
18  
19  
20  
21  
22  
23  
24  
25  
26  
27  
28  
29  
30  
31  
32  
33  
34  
35  
36  
37  
38  
39  
40  
41  
42  
43  
44  
45  
46  
47  
48  
49  
50  
51  
52  
53  
54  
55  
56  
57  
58  
59  
60

(c)



**Figure 7.** Contact schema between the surfaces of rods with (a) low and (b) high peak densities and a smooth plane. (c) Surface with a high peak density and a long quasi-period of waviness in contact with the seal surface.

The findings of the current study are consistent with those of Salant et al. [22], who investigated the impact of the surface roughness on the fluid-proof ability of the contact between a reciprocating seal and sliding rod using the contact model developed by Greenwood and Williamson [23]. Salant et al.'s model demonstrates the evolution of the fluid flow and sliding speed according to an a-dimensional parameter that matches the contact surface roughness ( $\hat{\sigma}$ ). This parameter is the root mean square roughness of the sealing element. According to Salant et al, if  $\hat{\sigma}$  is less than or equal to 2.7, the contact is fluid-proof.

$$\hat{\sigma} = \sigma R^{1/3} \eta^{2/3}$$

Rms roughness of sealing element definition from Salant et al. [22]

R is the radius of asperity defined by Greenwood and Williamson [23], and  $\sigma$  represents the surface root mean square average of the profile height deviations.  $\eta$  is the density of asperity on the surface; this parameter can be assimilated with the density of peaks Sds (number of peaks per square millimeter), which corresponds to the most relevant parameter for discriminating leakage.

Understanding every parameter that makes up  $\hat{\sigma}$  will allow the impact of its evolution on the surface morphology to be deduced. Johnson and Greenwood [24] defined the parameters  $\eta$ ,  $\beta$ , and  $\sigma$  as dependent:

$$\eta \sigma_* \beta = \text{constant} \quad (1)$$

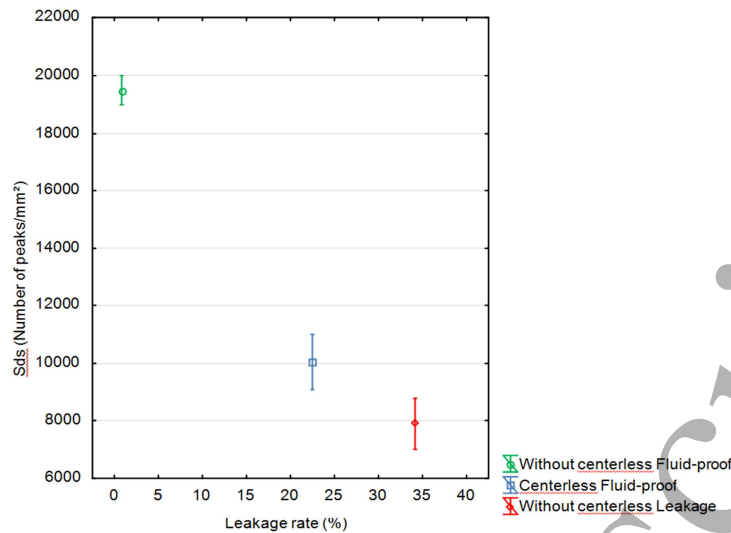
They empirically determined a constant value of 0.05 for bead blasted surfaces and defined  $\sigma_*$  by using Whitehouse and Archard's relation [25]:

$$\sigma_* = 0.7\sigma \quad (3)$$

$\hat{\sigma}$  is described as follows:

$$\hat{\sigma} = \alpha \beta^{-1} \eta^{-\frac{1}{3}} R^{\frac{1}{3}}, \quad \sigma = \frac{\alpha}{\beta \eta}, \quad \alpha = \text{constant} \quad (4)$$

According to (4), if  $\hat{\sigma}$  decreases, the number of asperities  $\eta$  will increase, and the contact becomes fluid-proof.



**Figure 8.** Leakage rate according to Sds for each type of rod at 50% macroscopic contact

Consequently, when the number of asperities or Sds (number of peaks per square millimeter) increases, the contact becomes fluid-proof. This is in accordance with earlier observations in this study that showed the relevancy of Sds for discriminating the contact sealing performance. Figure 8 plots the calculated density of summits on large and high plateaus of fluid-proof rods tooled without centerless leakage. The density of summits was calculated by using the same area as for the other samples. The density of summits was higher on plateaus of fluid-proof samples tooled without centerless leakage. This indicates that the experimental results in this study indirectly demonstrate the same conclusion as Salant *et al.*'s model.

## 5. Conclusion

Three different machining methods were used to machine rods from painting pumps (CF, WF, and WL). All rods tooled without centreless grinding (W) presented shape defects uncontrolled that were during the machining process. Rods tooled by the third supplier showed a long quasi-period of waviness (WF), in contrast to the rods tooled by the second supplier (WL). When there was no long waviness period, increasing the peak density improved the sealing by increasing the contact area, which caused significant percolation between surfaces. The waviness induced by the machining without centreless grinding was orthogonal to the leakage direction. It provided barriers that counteracted the leakage by increasing the local contact area on top of the roughness localized on the long quasi-periodic waviness signal. Therefore, the contact became fluid-proof because of the improved percolation between surfaces. The density of summits Sds was the only parameter that allowed discrimination between leaking and fluid-proof rods; this may be because motif decomposition integrates the three topographical components: circularity (transverse long-wave roughness), longitudinal waviness, and roughness according to the Wolf pruning algorithm. Consequently, a machining process can be proposed that produces an ideal surface texture to make a contact fluid-proof.

The ideal surface has to contain a quasi-periodic signal with a low frequency that is much greater than the micro-roughness level and orthogonal to the leakage direction. This waviness signal can be created with an adequate machining technique. The finishing process should maximize the density of peaks without affecting the low-frequency signal, like pumice stone. After the grinding operation, a slight superfinishing operation on the very near surface can be performed to result in a surface more homogeneous on top of the peak roughness. A slight erosion of the roughness peaks does not impact the density of peaks and helps expand the contact area by homogenizing the local contact pressure [17].

## References

- [1] Nikas G K 2010 *Proceedings of the Institution of Mechanical Engineers, Part J: Journal of Engineering Tribology* **224-1** 1-23.
- [2] Nau B S 1999 *Proceedings of the Institution of Mechanical Engineers, Part J: Journal of Engineering Tribology* **213-3**, 215-226
- [3] Bhaumik S, Kumaraswamy A and Guruprasad S 2013 *Procedia Engineering* **64** 835-843.
- [4] Kanters AFC and Visscher M 1989 *Tribology Series* vol 14, ed D Dawson, Cm Taylor, M Godet, and D
- [5] Nikas, G. K. 2003 *Journal of Tribology* **125** 60-69
- [6] Crudu M, Fatu A, Hajjam M, and Cristescu C 2013 *Seal. Technol.* **2013** 8-11
- [7] Huang Y and Salant RF 2016 *Tribol. Int.* **95** 306-315
- [8] Navinšek B, Panjan P and Milošev I 1999 *Surface and Coatings Technology* **116** 476-487
- [9] Deltombe R, Kubiak KJ, and Bigerelle M 2014 *Scanning* **36** 150-60
- [10] Le Goïc G, Bigerelle M, Samper S, Favrelière H, and Pillet M 2015 *Mech. Syst. Signal Process.* **66-7** 437-57
- [11] Bigerelle M, Najjar D, Mathia T, Iost A, Coorevits T, and Anselme K 2013 *Tribol. Int.* **59** 190-202
- [12] Bigerelle M, Gautier A, and Iost A 2007 *Sens. Actuators B: Chem.* **126** 2007 126-37
- [13] Najjar D, Bigerelle M, and Iost A 2003 *Wear* **254** 450-60
- [14] Núñez PJ, Simão J, Rubio EM, and Rincón JL 2006 *Mater. Sci. Forum* **526** 127-32
- [15] ISO 16610-21 2011 *Geometrical Product Specifications (GPS) – Filtration – Part 21: Linear Profile Filters: Gaussian Filters* (Geneva: International Organization for Standardization)
- [16] ASME B46.1 2009 *Surface Texture: Surface Roughness* (New York: American Society of Mechanical Engineers)
- [17] Deltombe R, Bigerelle M, and Jourani A 2015 *Surf. Topogr. Metrol. Prop.* **4** 015003
- [18] Jourani A, Hagège B, Bouvier S, Bigerelle M, and Zahouani H 2013 *Tribol. Int.* **59** 30-7
- [19] Jourani A 2015 *Int. J. Surf. Sci. Eng.* **9** 231-46
- [20] Bottiglione F, Carbone G, and Mantriota G 2009 *Tribol. Int.* **42** 731-7
- [21] Papatheodorou T, and Hannifin P 2005 *Sealing Technology* **4** 5-10.
- [22] Salant RF, Maser N, and Yang B 2007 *Journal of Tribology* **129-1** 91-97
- [23] Greenwood JA, and Williamson JBP 1966 *Proceedings of the Royal Society of London A: Mathematical, Physical and Engineering Sciences* **295**(1442). The Royal Society
- [24] Johnson KL, Greenwood JA, and Poon, SY. 1972 *Wear* **19-1**, 91-108
- [25] Whitehouse D J, and Archard JF 1970 *Proceedings of the Royal Society of London A: Mathematical, Physical and Engineering Sciences* **316-1524** 97-121 The Royal Society

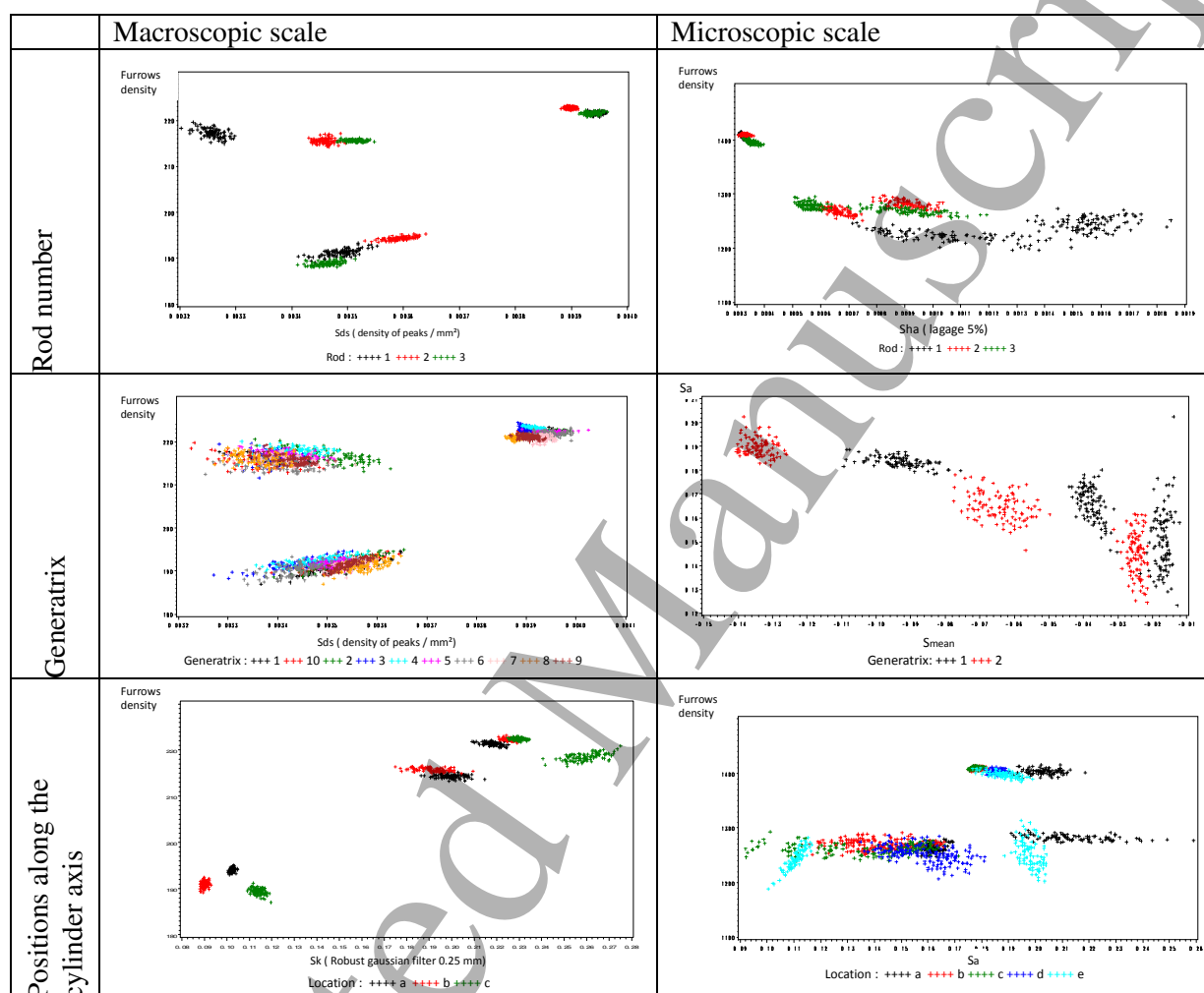
## APPENDIX A: Repeatability of measurements

The repeatability of results is important to confirming their reliability. The table below presents the repeatability of measurements.

Diagrams located in the first row of the table show the repeatability of measurements of the three rods studied for each rod type (CF, WF, WL) at the macroscopic and microscopic scales.

Diagrams located in the second row of the table show the repeatability of measurements around the axis at angle intervals of  $36^\circ$  (from 1 to 10) of each rod at the macroscopic and microscopic scales.

Diagrams located in the last row of the table show the repeatability of rod measurements along the cylinder axis at two (microscopic scale) or three (macroscopic scale) positions.



These charts confirm the repeatability of the measurements at the macroscopic and microscopic scales.